





Geophysical Research Letters[®]

RESEARCH LETTER

10.1029/2022GL100945

Intensification of the East Australian Current After ~1400 CE

Ruixiang Zhai¹, Mahyar Mohtadi^{2,3} , Andrew M. Dolman⁴ , Yusuke Yokoyama⁵ , and Stephan Steinke¹ 

Key Points:

- Mg/Ca-based sea surface temperature reconstructions reveal an intensification of the East Australian Current (EAC) after ~1400 CE
- A stronger EAC is likely driven by strengthening of the Southern Hemisphere subtropical gyre due to a Southern Annular Mode shift toward its positive phase
- More El Niño-like conditions may also strengthen the EAC by an equatorward shift of the South Equatorial Current bifurcation latitude

Supporting Information:

Supporting Information may be found in the online version of this article.

Correspondence to:

S. Steinke,
ssteinke@xmu.edu.cn

Citation:

Zhai, R., Mohtadi, M., Dolman, A. M., Yokoyama, Y., & Steinke, S. (2022). Intensification of the East Australian current after ~1400 CE. *Geophysical Research Letters*, 49, e2022GL100945. <https://doi.org/10.1029/2022GL100945>

Received 24 AUG 2022
Accepted 7 DEC 2022

Author Contributions:

Conceptualization: Mahyar Mohtadi, Stephan Steinke
Formal analysis: Ruixiang Zhai, Mahyar Mohtadi, Stephan Steinke
Funding acquisition: Mahyar Mohtadi, Stephan Steinke
Investigation: Ruixiang Zhai
Methodology: Ruixiang Zhai, Yusuke Yokoyama
Software: Andrew M. Dolman
Supervision: Stephan Steinke

© 2022. The Authors.

This is an open access article under the terms of the [Creative Commons Attribution-NonCommercial-NoDerivs License](https://creativecommons.org/licenses/by/4.0/), which permits use and distribution in any medium, provided the original work is properly cited, the use is non-commercial and no modifications or adaptations are made.

¹Department of Geological Oceanography, State Key Laboratory of Marine Environmental Science, College of Ocean and Earth Sciences, Xiamen University, Xiamen, China, ²MARUM-Center for Marine Environmental Sciences, University of Bremen, Bremen, Germany, ³Faculty of Geosciences, University of Bremen, Bremen, Germany, ⁴Helmholtz Centre for Polar and Marine Research, Alfred-Wegener-Institute, Potsdam, Germany, ⁵Department of Earth and Planetary Sciences, University of Tokyo, Tokyo, Japan

Abstract The East Australian Current (EAC) is the western boundary current of the South Pacific Subtropical Gyre that transports warm tropical waters to higher southern latitudes and significantly impacts the climate of Australia and New Zealand. Modern observations show that the EAC has strengthened with rising global temperatures. However, little is known about the pre-industrial variability of the EAC and the forcing mechanisms. Planktic foraminifera *Globigerinoides ruber* (white) Mg/Ca-based sea surface temperature reconstructions offshore northeastern Australia between 15° and 26°S reveal an increase by ~1.2°C after ~1400 CE. We infer that the increase in temperature is related to a stronger EAC heat transport that is likely driven by a strengthening of the Southern Hemisphere subtropical gyre circulation due to a progressive shift of the Southern annular mode toward its positive phase and of El Niño-Southern Oscillation toward more El Niño-like conditions.

Plain Language Summary The East Australian Current (EAC) transports large amounts of heat out of the Western Pacific Warm Pool into the subtropics and subpolar regions, thereby regulating the local and global climate. The few existing reconstructions of past changes in transport and temperature of the EAC are contradictory resulting in a knowledge gap in long-term variability of the southwest Pacific currents, which in turn hampers a reliable projection of future tropical and subtropical climate development. We use sea surface temperature reconstructions along the EAC path off northeastern Australia to estimate changes in the EAC heat transport over the past 4,000 years and its potential driving mechanisms. Our results reveal an increase in temperature after ~1400 CE, which we relate to an intensification of the EAC strength. The strengthening of the EAC after ~1400 CE is likely associated with a strengthening of the Southern Hemisphere subtropical gyre circulation due to a progressive shift of the Southern annular mode toward its positive phase and of El Niño-Southern Oscillation toward more El Niño-like conditions.

1. Introduction

The South Pacific poleward-flowing western boundary current (WBC)—the East Australian Current (EAC)—flows along the east coast of Australia and redistributes heat and moisture between the tropics and the mid-latitudes, and thus plays an important role in climate changes in the southwest Pacific. For example, the timing and intensity of EAC changes have been shown to influence both regional climates (e.g., Sprintall et al., 1995) and East Coast lows (severe weather events) along the east Australian coast (Hopkins & Holland, 1997). Specifically, a weaker EAC transport is linked to anomalous cool conditions in New Zealand (Sprintall et al., 1995), whereas a stronger EAC is shown to increase rainfall along the eastern Australian coast (Shi et al., 2008). Furthermore, the EAC also exerts a strong influence on the marine productivity offshore eastern Australia through formation of eddies and coastal upwelling (Roughan & Middleton, 2004; Schaeffer et al., 2014; Suthers et al., 2011). The EAC is the result of the bifurcation of the South Equatorial Current (SEC) between 13° and 25°S (Hu et al., 2015), when it collides with the Queensland Plateau (Ridgway & Dunn, 2003) (Figure S1 in Supporting Information S1). After its formation, the EAC follows the coastline until ~30°S, where the outflow of the EAC current separates and flows east across the Tasman Sea forming the Tasman Front (TF) (Andrews et al., 1980). A minor portion of the EAC continue to flow south along the Australian coast as EAC extension (Ridgway & Godfrey, 1994; Wyrski, 1962). The EAC is strongest during austral summer and weakens during the austral winter (Godfrey et al., 1980; Ridgway & Godfrey, 1997). A more recent study shows a maximum EAC transport of 21.6 ± 1.4 Sv at 26°S in March, and a minimum transport of 18 ± 1.4 Sv in August (Zilberman et al., 2018). Another study shows

Validation: Ruixiang Zhai, Mahyar Mohtadi, Andrew M. Dolman, Stephan Steinke

Visualization: Ruixiang Zhai, Mahyar Mohtadi, Stephan Steinke

Writing – original draft: Ruixiang Zhai, Mahyar Mohtadi, Andrew M. Dolman, Stephan Steinke

Writing – review & editing: Ruixiang Zhai, Mahyar Mohtadi, Andrew M. Dolman, Yusuke Yokoyama, Stephan Steinke

significant annual variability of the poleward transport between 28°S and 39°S (Cetina-Heredia et al., 2015). This is partly attributed to the seasonal movement of the SEC bifurcation latitude (SBL) controlled by seasonal wind stress curl variability (i.e., the seasonal shift of trade winds) (Hu et al., 2015). The SBL shifts northward toward the equator in austral summer and southward in austral winter (Chen & Wu, 2015; Kessler & Gourdeau, 2007). When the SEC is closer to the equator, the EAC transport is strengthened (Kessler & Gourdeau, 2007). The stronger EAC flow in summer is associated with higher eddy kinetic energy (EKE) in the Tasman Sea (Qiu & Chen, 2004) and a poleward shift in the separation latitude of the EAC (Ypma et al., 2016). El Niño–Southern Oscillation (ENSO) influences the SBL and thus controls the inter-annual heat transport variability of the EAC in a similar way. During El Niño (La Niña) conditions, the SEC bifurcates at a more equatorward (poleward) latitude leading to a stronger (weaker) EAC transport (Hu et al., 2015). ENSO may also influence the EAC transport by changes in the strength of the SEC. Kessler and Cravatte (2013) show that the westward transport of SEC entering the Coral Sea increases after an El Niño year and decreases following a La Niña year. In addition, Fort Denison tide-gauge data in Sydney Harbor, Australia, show that interannual to decadal variations in observed sea level data, which are influenced by multi-year variability in ENSO over previous years with an approximate 3-year lag are strongly connected to variations of the EAC transport (Holbrook et al., 2011). Modern variability in EAC strength is also strongly controlled by the Southern Annular Mode (SAM) on annual to decadal timescales (SAM; e.g., Cai, 2006; Cai et al., 2005; Hill et al., 2008, 2011). During positive SAM phases, the EAC transports more tropical/subtropical water into the southwest Pacific (Cai, 2006; Cai et al., 2005; Hill et al., 2008, 2011; Roemmich et al., 2016).

Historical sea surface temperature (SST) data show a surface water warming off the coast of Queensland since the late 1800s with an increase of ~1°C over the past 100 years, with most of the increase (about 0.6°C) taking place since the 1960s (Bustamante et al., 2012), which is associated with an increase in the strength of the EAC. Likewise, observations from a long-term coastal station off eastern Tasmania show that the EAC has strengthened and extended further southward between 1944 and 2002 (Ridgway, 2007). As a result, the south Tasman Sea region has become both warmer and saltier during this period, which corresponds to a poleward advance of the EAC extension of about 350 km (Ridgway, 2007). There is a strong consensus in climate model simulations that those trends will continue and accelerate over the next 100 years (Ridgway & Hill, 2009). In addition, ocean-atmosphere coupled climate models suggest a stronger EAC extension in the future (Sen Gupta et al., 2016; Wang et al., 2014; Yang et al., 2016). Climate projections show that this strengthening of the EAC is driven by a spin-up and southward shift of the entire Southern Hemisphere subtropical ocean circulation. The EAC is predicted to both strengthen and warm significantly (Cai et al., 2005). Changes in Southern Hemisphere subtropical gyre are linked to an intensification of the wind stress curl over a broad region of the South Pacific arising from an intensification and poleward shift in the circumpolar westerly winds because of an upward trend of the Southern Annular Mode (SAM) (Cai et al., 2005; Gillett & Thompson, 2003). A positive SAM also drives a poleward shift of the mid-latitude easterly winds, which is described as the main cause of the poleward movement of the EAC (and its bifurcation latitude) in the past few decades (Li et al., 2022). The poleward movement of the EAC led to an increase in eddy activity, which explains most of the 20th warming trend and the southward advance of the EAC extension (Li et al., 2022). Modern observations also show that the enhanced wind stress curl results in a southward expansion of the subtropical gyre, a stronger EAC extension but in a weaker Tasman Front on decadal scales, highlighting the complexity of this WBC system (Hill et al., 2011). Recent studies suggest that the poleward shift and/or intensification of the WBCs and poleward shift of the major ocean gyres over the last century are likely a global phenomenon over most ocean basins (Wu et al., 2012; Yang et al., 2016, 2020).

However, less is known about pre-industrial variability of the EAC and its driving mechanisms. A deep sea sediment core study from the East Tasman Plateau reveals that the EAC has not reached the core site during glacial periods but was present east of Tasmania during all interglacial periods over the last ~460 ka (De Deckker et al., 2019). Likewise, generally warmer surface water conditions in the Southwest Pacific during the peak interglacial Marine Isotope Stage 5e, especially in the western Tasman Sea are interpreted to reflect a strengthened EAC, which likely extended the subtropical influence to ~45°S off Tasmania (Cortese et al., 2013). A study on fossil corals from the Great Barrier Reef suggests that the Last Glacial Maximum and the last deglaciation were characterized by a considerably steeper meridional SST gradient in the western Coral Sea than today (Felix et al., 2014). A steeper meridional SST gradient implies a relatively weaker EAC and a northward expansion of cooler subtropical and subantarctic waters. These interpretations are in good agreement with stable oxygen isotope results in sediment cores from the Coral Sea and Tasman Sea, which indicate that the EAC separation

(presently south of $\sim 30^{\circ}\text{S}$) shifted northward to between $\sim 23^{\circ}$ and $\sim 26^{\circ}\text{S}$ during the last glacial period (Bostock et al., 2006). Multicentennial-scale, high resolution records of subsurface water radiocarbon reservoir ages from black corals off the coast of southeast Australia and northern New Zealand reveal a weaker EAC extension and stronger TF during the Little Ice Age (LIA) (Hitt et al., 2022; Komugabe-Dixson et al., 2016). In this context, past records of multi-decadal to centennial-scale changes in transport and temperature of the EAC are crucial for a deeper understanding of the natural variability of the EAC, which could provide further insight into the variability of major ocean gyres in the context of present and future climate change. To this end, we reconstruct the SST along the EAC path between 15°S and 26°S off northeastern Australia in order to estimate changes in the EAC transport over the past 4,000 years and their potential driving mechanisms.

2. Material and Methods

The analyzed sediment cores (GeoB22202-1, $26^{\circ}07.818'\text{S}$, $153^{\circ}59.366'\text{E}$, water depth 965 m; GeoB22222-1, $17^{\circ}17.698'\text{S}$; $146^{\circ}56.354'\text{E}$, water depth 1,168 m; GeoB22230-2, $15^{\circ}26.473'\text{S}$, $145^{\circ}52.198'\text{E}$, water depth 968 m) were recovered by using a multicorer during R/V SONNE cruise SO-256 in the Coral Sea, offshore NE Australia in 2017 (Mohtadi et al., 2017) (Figure S1 in Supporting Information S1). The recovered sediments are classified as nanofossil mud rich in planktic foraminifera and foraminifera-bearing nanofossil ooze, respectively (Mohtadi et al., 2017). Pteropods are present with high abundances, indicating a good aragonite/calcite preservation throughout the cores.

The age model of the multi-cores is based on Accelerator Mass Spectrometry (AMS) radiocarbon dates. AMS radiocarbon dating was performed on monospecific samples of planktic foraminifera *Trilobatus sacculifer* (Table S1 in Supporting Information S1). Due to the lack of sufficient specimens for monospecific foraminifera samples, one dating of core GeoB22202-1 (0.5 cm core depth) was obtained on a mixed sample of *Globigerinoides ruber* (white) and *T. sacculifer* (see Table S1 in Supporting Information S1). *G. ruber* (white) ranges among the shallowest dwelling planktic foraminifera out of all modern species with a mixed layer habitat (0–80 m), whereas *T. sacculifer* lives at bottom of mixed layer and uppermost thermocline conditions (45–85 m) in the western Pacific (e.g., Hollstein et al., 2017). Restricting dating to species with relatively narrow and shallow depth ranges (e.g., *G. ruber*, *T. sacculifer*) rather than those known to migrate to greater depths during the life cycle (e.g., *Neogloboquadrina dutertrei*) provide more accurate (and slightly younger) ages as they are less affected by deeper, older waters. Radiocarbon ages were measured at the Analytical Center for Environmental Science, Atmosphere and Ocean Research Institute, University of Tokyo, Japan. Each radiocarbon date was individually calibrated into calendar years with RBAcon (Blaauw & Christen, 2011) using the Marine20 calibration curve (Heaton et al., 2020) and applying a local reservoir age correction of $\Delta R = -155 \pm 13$ years (Druffel & Griffin, 1999; Hua et al., 2015; Ulm, 2002). As the GeoB22202-1 *G. ruber*/*T. sacculifer* sample at 0.5 cm contains excess ^{14}C , probably from mid-20th century atmospheric thermonuclear weapons tests, the online version of the software program CALIBomb (Reimer & Reimer, 2022) was used for the conversion of this sample to calendar ages. A continuous depth-age model was derived with the same Bayesian approach using RBAcon (see above) (Blaauw & Christen, 2011). The depth-age models of the three multiple cores used in this study (GeoB22202-1, GeoB22222-1, GeoB22230-2) are given in Figure S2 in Supporting Information S1. Based on the age models, the multiple cores GeoB22202-1 and GeoB22230-2 cover the last $\sim 1,000$ years and $\sim 1,300$ years, respectively. Core GeoB22222-1 covers the time interval ~ 1870 BCE to ~ 1023 CE. Sedimentation rates range between 25 cm/ka to 29.4 cm/ka in core GeoB22202-1, between 4.6 cm/ka to 7.5 cm/ka in core GeoB22222-1, and between 12.7 cm/ka to 16.4 cm/ka in GeoB22230-2.

Mg/Ca analyses on *G. ruber* (white) were performed on approximately 30 specimens of the 250–355 μm size fraction. The foraminiferal tests were cleaned following the cleaning protocol developed by Barker et al. (2003). After cleaning, the dissolved samples were centrifuged (10 min at 6,000 rpm), transferred into test tubes and diluted and analyzed with an Inductively Coupled Plasma Optical Emission Spectrophotometer (ICP-OES; Agilent 5110 VDV) at the Center of Major Equipment and Technology of the State Key Laboratory of Marine Environmental Science (MEL). After every fifth sample, an internal standard (Mg/Ca = 4.12 mmol/mol) was run to monitor the instrumental precision. The relative standard deviation of the in-house standard was 0.04 mmol/mol over the measurement period of the three multiple cores. Replicate measurements of re-picked samples of cores GeoB22202-1 ($n = 48$), GeoB22222-1 ($n = 47$) and GeoB22230-2 ($n = 56$) revealed an average standard deviation for Mg/Ca of 0.14 mmol/mol, 0.16 mmol/mol and 0.22 mmol/mol, respectively. Al/Ca, Mn/Ca and

Fe/Ca were determined along with Mg/Ca to assess the efficacy of the cleaning procedure that is, the removal of clays, and the occurrence of syn-sedimentary and post-depositional precipitated Fe-Mn-oxyhydroxides and Fe-Mn carbonate coatings, respectively. Aluminum was found to be under the detection limit of the ICP-OES technique and the Fe/Ca and Mn/Ca ratios of samples from the three multiple cores are lower than the 0.1 mmol/mol indicating clean, uncontaminated foraminiferal tests (Barker et al., 2003). The Mg/Ca ratios are thus not affected by clay minerals or by syn-sedimentary and post-depositional precipitated Fe-Mn-oxyhydroxides and Fe-Mn carbonate coatings. SST estimates in °C for *G. ruber* were obtained by using the species-specific equation of Anand et al. (2003) ($\text{Mg/Ca (mmol/mol)} = 0.34 \exp(0.102 \times T(^{\circ}\text{C}))$). We selected this calibration equation because the derived core top temperatures are closest to the annual average temperatures of the Extended Reconstructed Sea Surface Temperature record for the time period 1854 to 1900 (B. Y. Huang et al., 2017). To estimate errors for the temperature reconstructions, we used a numerical method that propagates the Mg/Ca measurement error and the uncertainty from the Mg/Ca temperature calibration. We refit the calibration regression model using the original species specific data from Anand et al. (2003) and extracted the variance-covariance matrix of the intercept and slope parameters. With this we then randomly sampled 1,000 pairs of calibration parameters. For each Mg/Ca measurement we then created 1,000 random normally distributed measurement error values, with mean equal to the measured value and standard deviation equal to the core-specific measurement errors estimated above. These were then calibrated to temperature and the standard deviation across samples of each original value is its corresponding error estimate. The resulting error estimates were 0.39°C, 0.47°C, and 0.56°C for GeoB22202-1, GeoB22222-1, and GeoB22230-2, respectively. In order to estimate the timing of transitions in our SST records, we fitted continuous piecewise regression lines with a single breakpoint through our planktic foraminiferal Mg/Ca-based SST data, using the R package “segmented” (Muggeo, 2008) (Figures 2a and 2b).

3. Results and Discussion

3.1. Mg/Ca Palaeothermometry and SST Variability in the Coral Sea

Mg/Ca ratios of *G. ruber* (white) vary between 4.4 mmol/mol and 5.0 mmol/mol and the estimated Mg/Ca surface water temperatures range from 25.1°C to 26.4°C at southern site GeoB22202-1 (Figure S1 in Supporting Information S1). At the two northern sites, the Mg/Ca ratios vary between 5.1 mmol/mol and 5.4 mmol/mol and the inferred Mg/Ca water temperatures range from 26.5°C to 27.11°C at GeoB22222-1 (Figure 1; Data Set S1 in Supporting Information S1).

The Mg/Ca ratios vary between 5.2 mmol/mol and 5.8 mmol/mol and the estimated Mg/Ca water temperatures range from 26.6°C to 27.8°C at GeoB22230-2 (Figure 1a). The reconstructed Mg/Ca-based SSTs reveal relatively stable and less variable SST values over the period ~1900 BCE to ~1400 CE and a prominent increase in SSTs at both cores GeoB22202-1 and GeoB22230-2 off eastern Australia thereafter. In order to better constrain the onset of this warming, we performed a statistical analysis of breakpoints in the SSTs using the R package “segmented” (Muggeo, 2008) (see also above). For the southern core GeoB22202-1 and northern core GeoB22230-2, breakpoints were identified at 1097 CE \pm 40 years (1 σ error) and 1393 CE \pm 102 years (1 σ error), respectively (Figure 2a). The single breakpoint models are highly significant when tested against a linear model by *F* test ($p < 0.001$). By combining the SST data from the southern core GeoB22202-1 and the northern core GeoB22230-2 and subtracting their respective mean values where they overlap, a breakpoint is identified at 1396 CE \pm 61 years (1 σ error), which is significant when tested against a linear model by *F* test ($p < 0.001$) (Figure 2b).

By combining the SST data from the three cores by subtracting their respective mean values where they overlap, a breakpoint is identified at 1385 CE \pm 57 years (1 σ error), which is again significant when tested against a linear model by *F* test ($p < 0.001$; Figure 1c). Our reconstructed SST records do not reveal any centennial-scale warm and cold periods associated with European/North Atlantic climate anomalies termed the Medieval Warm Period (MWP; ~950–1250 CE) and the LIA (~1400–1850 CE). Our temperature reconstructions are also in marked contrast to those of combined land and ocean temperature records of Australasia for the last millennium, which reveal a pronounced cool period consistent with the timing of the North Atlantic/Northern Hemisphere LIA (Gergis et al., 2016) (Figure 2f). In contrast, land surface temperature reconstructions of Australia as inferred from borehole temperatures over the past 2000 years reveal a LIA cooling in southern Australia and Victoria (southeastern SE Australia) but no cooling during the LIA in northeastern Queensland (for borehole sites see Figure S1 in Supporting Information S1; for temperature record see Figure 2e) (Suman et al., 2018) consistent

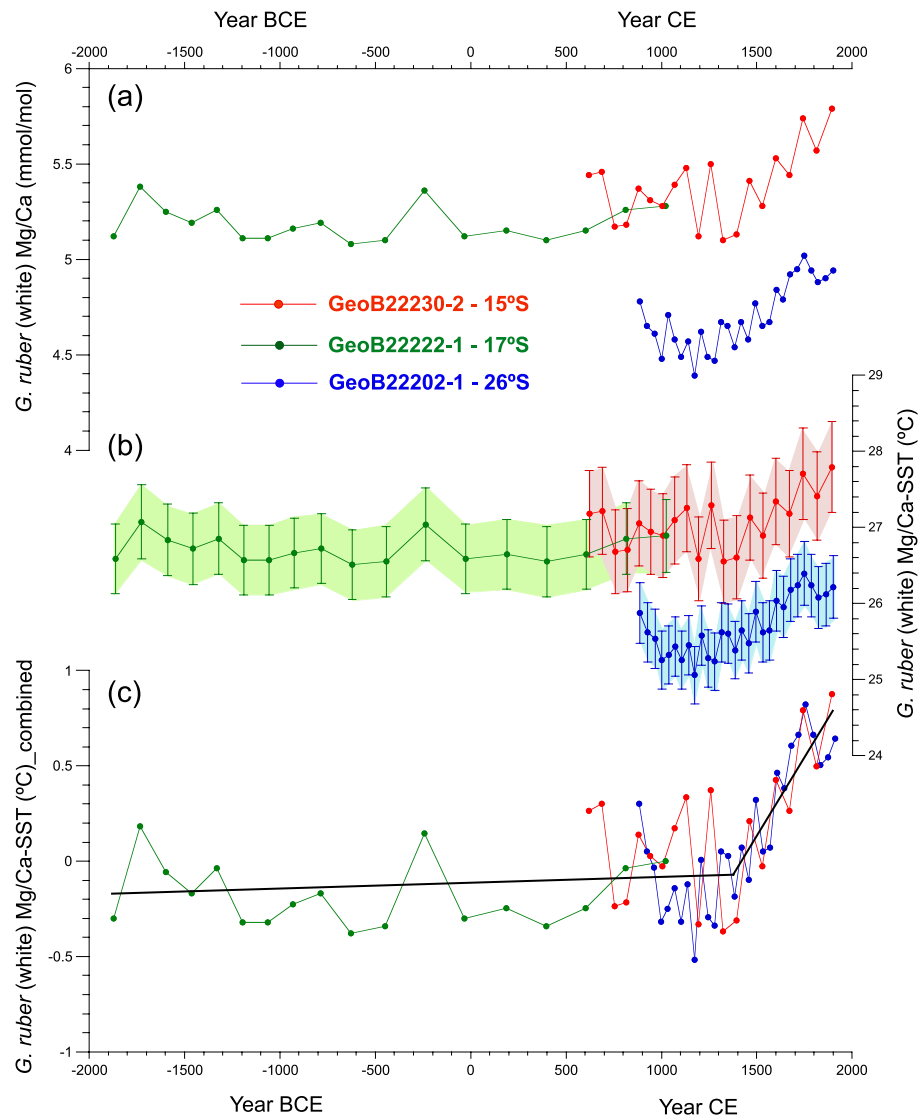


Figure 1. Reconstructed SST in the Coral Sea over the past 4,000 years. (a) Shell Mg/Ca of planktic foraminifera *Globigerinoides ruber* (white) in multi-cores GeoB22202-1 (blue), GeoB22222-1 (green) and GeoB22230-2 (red) and the calculated SST (b). Error bars and envelopes in (b) indicate 1σ errors. (c) Combined SST data of multi-cores GeoB22202-1, GeoB22222-1 and GeoB22230-2 by subtracting their respective mean values where the three records overlap. The black line indicates a breakpoint at $1385 \text{ CE} \pm 57$ years for the combined data.

with our SST reconstruction off northeastern Australia (Figure 2b). In addition, SST reconstructions based on coral Sr/Ca (Hendy et al., 2002) and sclerosponge stable oxygen isotopes (Wörheide, 1998) from the Great Barrier Reef (see Figures 2c and 2d) shows a similar SST trend as revealed by our SST reconstructions. We therefore suggest that the SST variability in the Coral Sea is driven by local and regional Southern Hemisphere changes rather than being remotely controlled by North Atlantic/Northern Hemisphere climate anomalies, which is in good agreement with the inferred non-coherence of global warm and cold periods during the preindustrial Common Era (Neukom et al., 2019).

3.2. Controls on SST Changes in the Coral Sea Over the Past 4,000 Years

Modern observations reveal that seasonal SST variability along the east coast of Australia is predominantly controlled by changes in the strength of the EAC (see above) (e.g., Bustamante et al., 2012; Ridgway, 2007). Our reconstructed Mg/Ca-based SSTs reveal relatively stable and less variable SSTs over the period ~ 1900 BCE

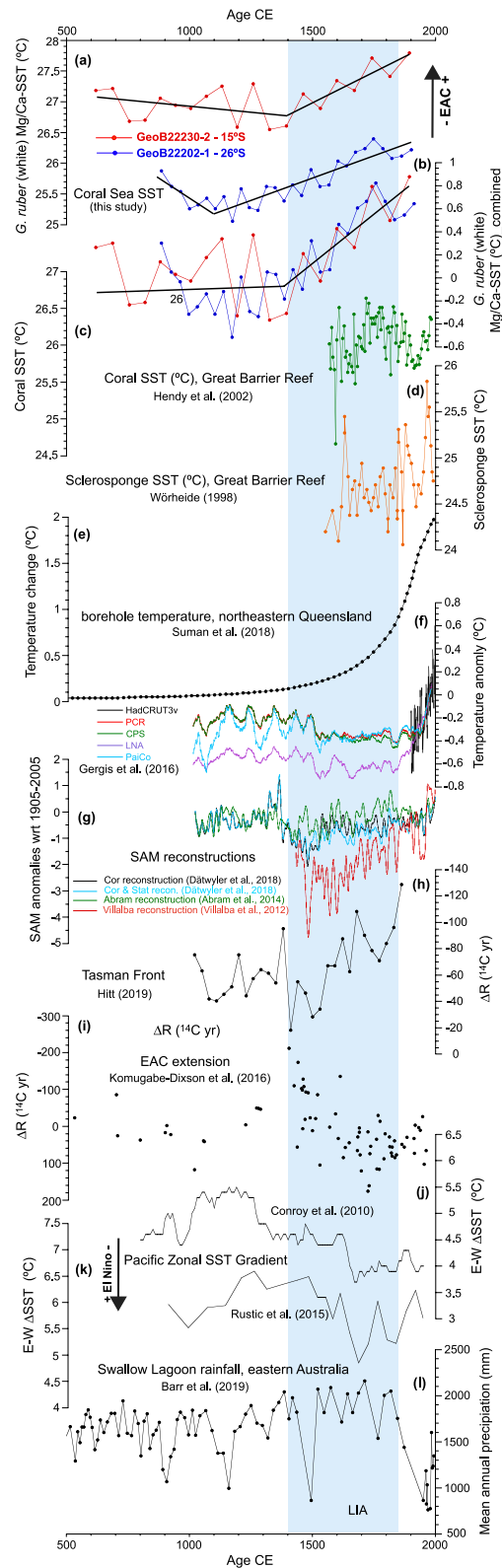


Figure 2.

to ~1400 CE in the northern Coral Sea. A prominent increase occurred after around ~1400 CE (Figure 2b). Although an SST record reaching back to ~1900 BCE is not available for our southern location, the same prominent increase in SST at around ~1400 CE is observed at ~26°S. We suggest that the consistent increase in SSTs along the northeastern coast of Australia indicates a stronger EAC heat transport after ~1400 CE because a stronger EAC can transport more warm tropical water and heat into the Coral Sea. Model simulations suggest an intensification of the EAC, which is likely driven by a “spin-up” and southward shift of the Southern Hemisphere subtropical ocean circulation during anthropogenic global warming (Cai, 2006; Cai et al., 2005). Changes in the South Pacific Subtropical Gyre strength are linked to changes in wind stress curl over a broad region of the South Pacific (Cai et al., 2005). Oceanic changes are forced by an intensification of the wind stress curl arising from a poleward shift in the circumpolar westerly winds due to a progressive shift of the SAM toward its positive phase (Cai et al., 2005; Gillett & Thompson, 2003). Based on those studies, we suggest that an intensification of the EAC after ~1400 CE is likely related to an upward trend of the SAM. Although the factors influencing past SAM variations are still debated, the increase in SST and thus EAC strength off the coast of northeastern Australia at our coring sites and thus EAC strength is consistent with a progressive shift of the SAM from a negative phase to a positive phase after ~1400 CE based on SAM index reconstructions (Abram et al., 2014; Dätwyler et al., 2018; Villalba et al., 2012) (Figure 2g). Like in modern climatology and model simulations, our data thus seem to indicate a close relationship between changes in EAC strength and SAM.

High-resolution record of subsurface water radiocarbon reservoir ages from black corals reveal a weaker EAC extension (Komugabe-Dixson et al., 2016), whereas black coral data off New Zealand suggest a stronger TF (Hitt et al., 2022) after ~1500 CE (Figures 2h and 2i), which is attributed to a weaker EAC under a negative SAM phase and/or La Niña conditions, resulting in a weaker EAC extension and a stronger TF. This interpretation is however significantly different to our interpretation of a strengthened EAC after ~1400 CE associated with a progressive shift of the SAM toward its positive phase and of ENSO toward more El Niño-like conditions (see below). An alternative explanation for these contrasting patterns is that the increase in surface water radiocarbon reservoir ages in the EAC extension region and decreased values off New Zealand area, is associated with changes in eddy activity as the SAM shift toward its positive phase. The EAC downstream area (EAC extension and TF) is a highly energetic area rich in dynamic mesoscale eddies (Malan et al., 2020; Schiller et al., 2008; Suthers et al., 2011) and coastal upwelling (Z. Huang & Wang, 2019). Modern observational studies have shown that the strength of the EAC extension is positively correlated with eddy-driven transport (Cetina-Heredia et al., 2014) and local upwelling events (Z. Huang & Wang, 2019; Schaeffer et al., 2014). In a recent study, Li et al. (2022) show that a positive shift of SAM drives a poleward shift of the mid-latitude easterly winds, which is regarded as the main cause of WBCs poleward movement in the past few decades. The poleward shift of the EAC results in an increase in eddy activity, which explains most of the warming trend and the southward advance of the EAC extension. Hence, a positive SAM shift after ~1400 CE would lead to an enhanced eddy activity in EAC extension, which might bring more “old” deep water into the subsurface layer. As for the TF, the ΔR decrease after ~1500 CE could also be explained by a weakening of TF associated with a decrease in eddy activity. This is supported by modern observations that the strength of the EAC extension and TF shows an anticorrelation on decadal time scales (Hill et al., 2011). In addition, model simulations reveal an increase of EKE in the EAC extension region and a decrease in the TF when compared to EKE changes between historical timescales (1860–1949) and projections (2061–2090), implying that the long-term trend in eddy activity may also show an anticorrelation between TF and EAC extension (Beech et al., 2022).

Figure 2. Comparison of the GeoB22202-1 and GeoB22230-2 SST records with other climate proxy records of the last 1,500 years. (a) *Globigerinoides ruber* (white) Mg/Ca-SST estimates of core GeoB22230-2 and GeoB22202-1 indicating changes in the strength of the EAC; (b) Combined SST data of multi-cores GeoB22202-1 and GeoB22230-2 by subtracting their respective mean values where both records overlap. Black lines indicate breakpoints for the southern core GeoB22202-1 and northern core GeoB22230-2 at 1097 CE \pm 40 years and 1393 CE \pm 102 years, respectively (a), and at 1396 CE \pm 61 years for the combined data (b). (c) SST reconstruction based on coral Sr/Ca at 18.33°S off eastern Australia (Hendy et al., 2002); (d) SST reconstruction based on sclerosponge stable oxygen isotopes (Wörheide, 1998); (e) Reconstructed ground surface temperature for northeastern Queensland from borehole temperature data (Suman et al., 2018); (f) 30-year-filtered Australasian temperature reconstruction based on Principle Component Regression (PCR; red curve), Composite Plus Scale (CPS; green curve), Bayesian Hierarchical Model (LNA; blue curve) and Pairwise Comparison (PaiCo; cyan curve) methods relative to the 1961–1990 base period. Mean SONDJF instrumental HadCRUT3v data averaged over the Australasian region for 1900–2014 (black line) (Gergis et al., 2016); (g) Southern Annular Mode (SAM) index reconstructions for the last 1,000 years (anomalies with respect to 1905–2005) (Abram et al., 2014; Dätwyler et al., 2018; Villalba et al., 2012); (h) 30-year-binned Tasman Front ΔR (^{14}C yr) (Hitt et al., 2022); (i) East Australian Current extension ΔR (^{14}C yr) (Komugabe-Dixson et al., 2016); (j) tropical Pacific zonal SST gradient (Conroy et al., 2010) and (k) zonal SST gradient between western Pacific warm Pool and eastern equatorial Pacific (Rustic et al., 2015) both indicating the state of the ENSO; and (l) mean annual precipitation of Swallow Lagoon in eastern Australia (Barr et al., 2019). Blue bar indicates the Little Ice Age (LIA).

Today, the EAC heat transport/strength is also sensitive to ENSO variability by changing the SBL (Hu et al., 2015). We therefore hypothesize that changes in the background state of the tropical Pacific, so-called “El Niño-like” or “La Niña-like” conditions, may have also substantially contributed to SST changes along the EAC path as observed in our records off the coast of northeastern Australia. Assuming that changes in the EAC strength are mainly forced by atmosphere-ocean circulation changes related to ENSO, our SST records suggest that the increase in SST might be related to the prevalence of an El Niño-like mean state after ~1400 CE (during the LIA; please see above). Reconstructions of global surface temperature patterns by Mann et al. (2009) find a tendency for El Niño-like conditions in the tropical Pacific during the LIA, which agrees well with coral-based SST reconstruction from Palmyra Island in the central equatorial Pacific (Cobb et al., 2003). In addition, zonal gradient reconstructions of the tropical Pacific SST (Conroy et al., 2010) (Figure 2j), upwelling reconstructions off the southern coast of Indonesia (Steinke et al., 2014) as well as composite stalagmite $\delta^{18}\text{O}$ records from the Asian-Australian monsoon region (Zhang et al., 2022) also suggest El Niño-like conditions during the LIA and La Niña-like conditions during the MWP. Reconstructed SST, ENSO activity, and the tropical Pacific zonal gradient for the eastern Pacific suggest a persistent La Niña-like mean state during ~1150–1500 CE (± 30 years) and a persistent El Niño-like mean state during ~1500–1850 CE (± 30 years) in the tropical Pacific (Rustic et al., 2015) (Figure 2k). We thus suggest that together with the spin-up of South Pacific Subtropical Gyre driven by the positive trend of the SAM, more El Niño-like conditions after ~1400 CE might shift the bifurcation latitude of SEC equatorward and/or promote the SEC transport and thus EAC heat transport. Instrumental climate data indicates however that the relationship between ENSO and SAM tends to more frequently favor a positive SAM phase during La Niña, and a negative SAM phase during El Niño, although other combinations tied to internal variability can (less frequently) occur (Fogt et al., 2011; Wilson et al., 2016), opposite to our interpretation of more positive SAM and more El Niño-like conditions after 1400 CE. Reconstructions and models indicate that this negative correlation appears to have existed back to 1400 CE but with occasionally periods of positive ENSO–SAM correlations in individual model simulations and in palaeoclimate reconstructions (Dätwyler et al., 2020), highlighting the complex interplay between SAM and ENSO in the past. The studies of Barr et al. (2019) on Swallow Lagoon sediments and Coates-Marnane et al. (2018) on Moreton Bay sediments located close to our sites indicate persistently higher rainfall over Eastern Australia during the LIA, which is inconsistent with a more El Niño-like mean state but consistent with a more positive SAM phase and La Niña-like mean state (Figure 2l). Higher rainfall in subtropical eastern Australia during the LIA is in good agreement with rainfall proxy records from the western and equatorial Pacific (Griffiths et al., 2016; Yan et al., 2011), which suggest La Niña-like conditions prevailing during the LIA. In contrast, tree ring data of eastern Australia reveal several dry periods during the 16th century (Cook et al., 2016). Irrespective whether the western Pacific was in a more El Niño-like or a more La Niña-like mean state during the LIA as revealed by the contrasting oceanic and terrestrial proxy records for changes in ENSO during this period, we suggest that higher rainfall in Eastern Australia during the LIA is dominated by the positive SAM phase induced stronger EAC heat transport rather than La Niña-like conditions at that time, as a stronger positive phase of the SAM and thus stronger EAC have shown to promote rainfall along the east Australia coast in modern climatology (Ho et al., 2012; Shi et al., 2008). Prior to 1400 CE, the SAM was also in a positive phase (Abram et al., 2014; Dätwyler et al., 2018; Villalba et al., 2012), which is however not reflected in increased SSTs at our sites. We hypothesize that a more dominant La Niña-like mean state as suggested by many studies (for references see above) for this period resulted in a more poleward latitudinal shift of the SEC bifurcation and thus a decrease in the EAC heat transport which may have masked any potential control of the SAM on the SST patterns in the Coral Sea. A dominant La Niña-like mean state may have outweighed the control of the SAM on the SST patterns in the Coral Sea prior to ~1400 CE, since the poleward shift of SBL would cause relative cooler water entering the Coral Sea, and thus weaken the influence of current velocity variation caused by circulation intensity on local SST.

4. Conclusion

High-resolution planktic foraminifera *Globigerinoides ruber* Mg/Ca-based SST reconstructions from three sediment cores that were retrieved along an N-S transect offshore northeastern Australia reflect multi-decadal to centennial-scale variations of the EAC heat transport over the past four millennia. Our results show an increase of ~1.2°C after ~1400 CE, which we relate to an intensification of the EAC strength. The strengthening of the EAC after ~1400 CE is likely dominated by a spin-up of the Southern Hemisphere subtropical gyre associated with a progressive shift of the SAM toward its positive phase. We also suggest that a shift from more La Niña-like

conditions to more El Niño-like conditions around 1400 CE also contributed to the strengthening of the EAC. Our results shed new light on the complex behavior of the EAC and its potential driving mechanisms of the pre-industrial period.

Data Availability Statement

The data of this manuscript are archived at PANGAEA and can be downloaded using the following link: <https://doi.pangaea.de/10.1594/PANGAEA.948831>.

Acknowledgments

This study is supported by the Fundamental Research Funds for the Central Universities (20720170071) through a grant to S. Steinke, and Federal Ministry of Education and Research (BMBF) funding of the R/V Sonne expedition SO256 (03G0256A) to M. Mohtadi. R. Zhai was supported by the Undergraduate Honors Program of Marine Sciences at Xiamen University. We thank Y. Chen (State Key Laboratory of Marine Environmental Science, Xiamen University) for her help with the trace element analyses. This manuscript benefitted from discussions with M. Hollstein. We thank G. Dunbar and two anonymous reviewers for their constructive criticisms that have helped to improve the manuscript.

References

- Abram, N. J., Mulvaney, R., Vimeux, F., Phipps, S. J., Turner, J., & England, M. H. (2014). Evolution of the southern annular mode during the past millennium. *Nature Climate Change*, 4(7), 564–569. <https://doi.org/10.1038/Nclimate2235>
- Anand, P., Elderfield, H., & Conte, M. H. (2003). Calibration of Mg/Ca thermometry in planktonic foraminifera from a sediment trap time series. *Paleoceanography*, 18(2). <https://doi.org/10.1029/2002pa000846>
- Andrews, J. C., Lawrence, M. W., & Nilsson, C. S. (1980). Observations of the Tasman Front. *Journal of Physical Oceanography*, 10(11), 1854–1869. [https://doi.org/10.1175/1520-0485\(1980\)010<1854:Ootf>2.0.Co;2](https://doi.org/10.1175/1520-0485(1980)010<1854:Ootf>2.0.Co;2)
- Barker, S., Greaves, M., & Elderfield, H. (2003). A study of cleaning procedures used for foraminiferal Mg/Ca paleothermometry. *Geochemistry, Geophysics, Geosystems*, 4(9). <https://doi.org/10.1029/2003gc000559>
- Barr, C., Tibby, J., Leng, M. J., Tyler, J. J., Henderson, A. C. G., Overpeck, J. T., et al. (2019). Holocene El Niño-Southern Oscillation variability reflected in subtropical Australian precipitation. *Scientific Reports-Uk*, 9(1), 1627. <https://doi.org/10.1038/s41598-019-38626-3>
- Beech, N., Rackow, T., Semmler, T., Danilov, S., Wang, Q., & Jung, T. (2022). Long-term evolution of ocean eddy activity in a warming world. *Nature Climate Change*, 12(10), 910–917. <https://doi.org/10.1038/s41558-022-01478-3>
- Blaauw, M., & Christen, J. A. (2011). Flexible paleoclimate age-depth models using an autoregressive gamma process. *Bayesian Analysis*, 6(3), 457–474. <https://doi.org/10.1214/ba/1339616472>
- Bostock, H. C., Opdyke, B. N., Gagan, M. K., Kiss, A. E., & Fifield, L. K. (2006). Glacial/interglacial changes in the East Australian current. *Climate Dynamics*, 26(6), 645–659. <https://doi.org/10.1007/s00382-005-0103-7>
- Bustamante, R. H., Skewes, T., Hobday, A., Williams, K. J., Dunlop, M., & Poloczanska, P. (2012). *Queensland's biodiversity under climate change: Coastal and marine ecosystems*. CSIRO. <https://doi.org/10.4225/08/584ee7e74170c>
- Cai, W. (2006). Antarctic ozone depletion causes an intensification of the Southern Ocean super-gyre circulation. *Geophysical Research Letters*, 33(3), L03712. <https://doi.org/10.1029/2005gl024911>
- Cai, W., Shi, G., Cowan, T., Bi, D., & Ribbe, J. (2005). The response of the Southern Annular Mode, the East Australian Current, and the southern mid-latitude ocean circulation to global warming. *Geophysical Research Letters*, 32(23), L23706. <https://doi.org/10.1029/2005gl024701>
- Cetina-Heredia, P., Roughan, M., van Sebille, E., & Coleman, M. A. (2014). Long-term trends in the East Australian Current separation latitude and eddy driven transport. *Journal of Geophysical Research: Oceans*, 119(7), 4351–4366. <https://doi.org/10.1002/2014jc010071>
- Cetina-Heredia, P., Roughan, M., van Sebille, E., Feng, M., & Coleman, M. A. (2015). Strengthened currents override the effect of warming on lobster larval dispersal and survival. *Global Change Biology*, 21(12), 4377–4386. <https://doi.org/10.1111/gcb.13063>
- Chen, Z. H., & Wu, L. X. (2015). Seasonal variation of the Pacific South Equatorial current bifurcation. *Journal of Physical Oceanography*, 45(6), 1757–1770. <https://doi.org/10.1175/Jpo-D-14-0085.1>
- Coates-Marnane, J., Olley, J., Tibby, J., Burton, J., Haynes, D., & Kemp, J. (2018). A 1500 year record of river discharge inferred from fluvial-marine sediments in the Australian subtropics. *Palaeogeography, Palaeoclimatology, Palaeoecology*, 504, 136–149. <https://doi.org/10.1016/j.palaeo.2018.05.019>
- Cobb, K. M., Charles, C. D., Cheng, H., & Edwards, R. L. (2003). El Niño/Southern Oscillation and tropical Pacific climate during the last millennium. *Nature*, 424(6946), 271–276. <https://doi.org/10.1038/nature01779>
- Conroy, J. L., Overpeck, J. T., & Cole, J. E. (2010). *El Niño/Southern Oscillation and changes in the zonal gradient of tropical Pacific sea surface temperature over the last 1.2 ka*. PAGES news.
- Cook, B. I., Palmer, J. G., Cook, E. R., Turney, C. S. M., Allen, K., Fenwick, P., et al. (2016). The paleoclimate context and future trajectory of extreme summer hydroclimate in eastern Australia. *Journal of Geophysical Research: Atmospheres*, 121(21), 12820–12838. <https://doi.org/10.1002/2016JD024892>
- Cortese, G., Dunbar, G. B., Carter, L., Scott, G., Bostock, H., Bowen, M., et al. (2013). Southwest Pacific Ocean response to a warmer world: Insights from Marine Isotope Stage 5e. *Paleoceanography*, 28(3), 585–598. <https://doi.org/10.1002/palo.20052>
- Dätwyler, C., Grosjean, M., Steiger, N. J., & Neukom, R. (2020). Teleconnections and relationship between the El Niño-Southern Oscillation (ENSO) and the southern annular mode (SAM) in reconstructions and models over the past millennium. *Climate of the Past*, 16(2), 743–756. <https://doi.org/10.5194/cp-16-743-2020>
- Dätwyler, C., Neukom, R., Abram, N. J., Gallant, A. J. E., Grosjean, M., Jacques-Coper, M., et al. (2018). Teleconnection stationarity, variability and trends of the Southern Annular Mode (SAM) during the last millennium. *Climate Dynamics*, 51(5–6), 2321–2339. <https://doi.org/10.1007/s00382-017-4015-0>
- De Deckker, P., Barrows, T. T., Stuut, J. B. W., van der Kaars, S., Ayres, M. A., Rogers, J., & Chaproniere, G. (2019). Land-sea correlations in the Australian region: 460 ka of changes recorded in a deep-sea core offshore Tasmania. Part 2: The marine compared with the terrestrial record. *Australian Journal of Earth Sciences*, 66(1), 17–36. <https://doi.org/10.1080/08120099.2018.1495101>
- Druffel, E. R. M., & Griffin, S. (1999). Variability of surface ocean radiocarbon and stable isotopes in the southwestern Pacific. *Journal of Geophysical Research*, 104(C10), 23607–23613. <https://doi.org/10.1029/1999jc900212>
- Felis, T., McGregor, H. V., Linsley, B. K., Tudhope, A. W., Gagan, M. K., Suzuki, A., et al. (2014). Intensification of the meridional temperature gradient in the Great Barrier Reef following the last glacial maximum. *Nature Communications*, 5(1), 4102. <https://doi.org/10.1038/ncomms5102>
- Fogt, R. L., Bromwich, D. H., & Hines, K. M. (2011). Understanding the SAM influence on the South Pacific ENSO teleconnection. *Climate Dynamics*, 36(7–8), 1555–1576. <https://doi.org/10.1007/s00382-010-0905-0>
- Gergis, J., Neukom, R., Gallant, A. J. E., & Karoly, D. J. (2016). Australasian temperature reconstructions spanning the last millennium. *Journal of Climate*, 29(15), 5365–5392. <https://doi.org/10.1175/Jcli-D-13-00781.1>

- Gillett, N. P., & Thompson, D. W. J. (2003). Simulation of recent Southern Hemisphere climate change. *Science*, 302(5643), 273–275. <https://doi.org/10.1126/science.1087440>
- Godfrey, J. S., Cresswell, G. R., Golding, T. J., Pearce, A. F., & Boyd, R. (1980). The separation of the East Australian current. *Journal of Physical Oceanography*, 10(3), 430–440. [https://doi.org/10.1175/1520-0485\(1980\)010<0430:Tsoatea>2.0.Co;2](https://doi.org/10.1175/1520-0485(1980)010<0430:Tsoatea>2.0.Co;2)
- Griffiths, M. L., Kimbrough, A. K., Gagan, M. K., Drysdale, R. N., Cole, J. E., Johnson, K. R., et al. (2016). Western Pacific hydroclimate linked to global climate variability over the past two millennia. *Nature Communications*, 7(1), 11719. <https://doi.org/10.1038/ncomms11719>
- Heaton, T. J., Khler, P., Butzin, M., Bard, E., Skinner, L. C., Austin, W. E. N., et al. (2020). MARINE20—THE marine radiocarbon age calibration curve (0–55,000 CAL BP). *Radiocarbon*, 62(4), 1–42. <https://doi.org/10.1017/rdc.2020.68>
- Hendy, E. J., Gagan, M. K., Alibert, C. A., McCulloch, M. T., Lough, J. M., & Isdale, P. J. (2002). Abrupt decrease in tropical Pacific Sea surface salinity at end of Little Ice Age. *Science*, 295(5559), 1511–1514. <https://doi.org/10.1126/science.1067693>
- Hill, K. L., Rintoul, S. R., Coleman, R., & Ridgway, K. R. (2008). Wind forced low frequency variability of the East Australia Current. *Geophysical Research Letters*, 35(8), L08602. <https://doi.org/10.1029/2007GL032912>
- Hill, K. L., Rintoul, S. R., Ridgway, K. R., & Oke, P. R. (2011). Decadal changes in the South Pacific western boundary current system revealed in observations and ocean state estimates. *Journal of Geophysical Research*, 116(C1), C01009. <https://doi.org/10.1029/2009jc005926>
- Hitt, N. T., Sinclair, D. J., Neil, H. L., Fallon, S. J., Komugabe-Dixson, A., Fernandez, D., et al. (2022). Natural cycles in south Pacific gyre strength and the southern annular mode. *Scientific Reports-Uk*, 12(1), 18090. <https://doi.org/10.1038/s41598-022-22184-2>
- Ho, M., Kiem, A. S., & Verdon-Kidd, D. C. (2012). The southern annular mode: A comparison of indices. *Hydrology and Earth System Sciences*, 16(3), 967–982. <https://doi.org/10.5194/hess-16-967-2012>
- Holbrook, N. J., Goodwin, I. D., McGregor, S., Molina, E., & Power, S. B. (2011). ENSO to multi-decadal time scale changes in East Australian Current transports and Fort Denison sea level: Oceanic Rossby waves as the connecting mechanism. *Deep-Sea Research Part II*, 58(5), 547–558. <https://doi.org/10.1016/j.dsr2.2010.06.007>
- Hollstein, M., Mohtadi, M., Rosenthal, Y., Moffa Sanchez, P., Oppo, D., Martínez Méndez, G., et al. (2017). Stable oxygen isotopes and Mg/Ca in planktic foraminifera from modern surface sediments of the Western Pacific Warm Pool: Implications for thermocline reconstructions. *Paleoceanography*, 32(11), 1174–1194. <https://doi.org/10.1002/2017PA003122>
- Hopkins, L. C., & Holland, G. J. (1997). The origin and evolution of low-level potential vorticity anomalies during a case of Tasman Sea cyclogenesis - Comments. *Tellus*, 49(3), 401–403. <https://doi.org/10.1034/j.1600-0870.1997.t01-2-00007.x>
- Hu, D. X., Wu, L., Cai, W., Gupta, A. S., Ganachaud, A., Qiu, B., et al. (2015). Pacific western boundary currents and their roles in climate. *Nature*, 522(7556), 299–308. <https://doi.org/10.1038/nature14504>
- Hua, Q., Webb, G. E., Zhao, J. X., Nothdurft, L. D., Lybolt, M., Price, G. J., & Opydyke, B. N. (2015). Large variations in the Holocene marine radiocarbon reservoir effect reflect ocean circulation and climatic changes. *Earth and Planetary Science Letters*, 422, 33–44. <https://doi.org/10.1016/j.epsl.2015.03.049>
- Huang, B. Y., Thorne, P. W., Banzon, V. F., Boyer, T., Chepurin, G., Lawrimore, J. H., et al. (2017). Extended reconstructed sea surface temperature, version 5 (ERSSTv5): Upgrades, validations, and intercomparisons. *Journal of Climate*, 30(20), 8179–8205. <https://doi.org/10.1175/Jcli-D-16-0836.1>
- Huang, Z., & Wang, X. H. (2019). Mapping the spatial and temporal variability of the upwelling systems of the Australian south-eastern coast using 14-year of MODIS data. *Remote Sensing of Environment*, 227, 90–109. <https://doi.org/10.1016/j.rse.2019.04.002>
- Kessler, W. S., & Cravatte, S. (2013). ENSO and short-term variability of the south equatorial current entering the Coral Sea. *Journal of Physical Oceanography*, 43(5), 956–969. <https://doi.org/10.1175/Jpo-D-12-0113.1>
- Kessler, W. S., & Gourdeau, L. (2007). The annual cycle of circulation of the southwest subtropical Pacific, analyzed in an ocean GCM. *Journal of Physical Oceanography*, 37(6), 1610–1627. <https://doi.org/10.1175/Jpo3046.1>
- Komugabe-Dixson, A. F., Fallon, S. J., Eggins, S. M., & Thresher, R. E. (2016). Radiocarbon evidence for mid-late Holocene changes in south-western Pacific Ocean circulation. *Paleoceanography*, 31(7), 971–985. <https://doi.org/10.1002/2016pa002929>
- Li, J. D., Roughan, M., & Kerry, C. (2022). Drivers of ocean warming in the western boundary currents of the Southern Hemisphere. *Nature Climate Change*, 12(10), 901–909. <https://doi.org/10.1038/s41558-022-01473-8>
- Malan, N., Archer, M., Roughan, M., Cetina-Heredia, P., Hemming, M., Rocha, C., et al. (2020). Eddy-driven cross-shelf transport in the East Australian current separation zone. *Journal of Geophysical Research: Oceans*, 125(2), e2019JC015613. <https://doi.org/10.1029/2019JC015613>
- Mann, M. E., Zhang, Z. H., Rutherford, S., Bradley, R. S., Hughes, M. K., Shindell, D., et al. (2009). Global signatures and dynamical origins of the little ice age and medieval climate anomaly. *Science*, 326(5957), 1256–1260. <https://doi.org/10.1126/science.1177303>
- Mohtadi, M., Beaman, R. J., Boehnert, S., Daumann, M., Floren, V. M., Gould, J. L. A., et al. (2017). R/V SONNE cruise report SO256, TACTEAC, temperature and circulation history of the East Australian Current, Auckland (New Zealand)—Darwin (Australia), 17 April–09 May 2017.
- Muggeo, V. M. R. (2008). Segmented: An R package to fit regression models with broken-line relationships.
- Neukom, R., Steiger, N., Gomez-Navarro, J. J., Wang, J., & Werner, J. P. (2019). No evidence for globally coherent warm and cold periods over the preindustrial Common Era. *Nature*, 571(7766), 550–554. <https://doi.org/10.1038/s41586-019-1401-2>
- Qiu, B., & Chen, S. M. (2004). Seasonal modulations in the eddy field of the South Pacific Ocean. *Journal of Physical Oceanography*, 34(7), 1515–1527. [https://doi.org/10.1175/1520-0485\(2004\)034<1515:Smitef>2.0.Co;2](https://doi.org/10.1175/1520-0485(2004)034<1515:Smitef>2.0.Co;2)
- Reimer, R. W., & Reimer, P. J. (2022). CALIBomb [WWW program]. Retrieved from <http://calib.org>
- Ridgway, K. R. (2007). Long-term trend and decadal variability of the southward penetration of the East Australian Current. *Geophysical Research Letters*, 34(13). <https://doi.org/10.1029/2007gl030393>
- Ridgway, K. R., & Dunn, J. R. (2003). Mesoscale structure of the mean East Australian Current System and its relationship with topography. *Progress in Oceanography*, 56(2), 189–222. [https://doi.org/10.1016/S0079-6611\(03\)00004-1](https://doi.org/10.1016/S0079-6611(03)00004-1)
- Ridgway, K. R., & Godfrey, J. S. (1994). Mass and heat budgets in the East Australian current: A direct approach. *Journal of Geophysical Research*, 99(C2), 3231–3248. <https://doi.org/10.1029/93JC02255>
- Ridgway, K. R., & Godfrey, J. S. (1997). Seasonal cycle of the East Australian current. *Journal of Geophysical Research*, 102(C10), 22921–22936. <https://doi.org/10.1029/97jc00227>
- Ridgway, K. R., & Hill, K. (2009). The East Australian current. In *A marine climate change impacts and adaptation report card for Australia 2009*.
- Roemmich, D., Gilson, J., Sutton, P., & Zilberman, N. (2016). Multidecadal change of the south Pacific gyre circulation. *Journal of Physical Oceanography*, 46(6), 1871–1883. <https://doi.org/10.1175/jpo-d-15-0237.1>
- Roughan, M., & Middleton, J. H. (2004). On the East Australian current: Variability, encroachment, and upwelling. *Journal of Geophysical Research*, 109(C7), C07003. <https://doi.org/10.1029/2003jc001833>

- Rustic, G. T., Koutavas, A., Marchitto, T. M., & Linsley, B. K. (2015). Dynamical excitation of the tropical Pacific Ocean and ENSO variability by little ice age cooling. *Science*, 350(6267), 1537–1541. <https://doi.org/10.1126/science.aac9937>
- Schaeffer, A., Roughan, M., & Wood, J. E. (2014). Observed bottom boundary layer transport and uplift on the continental shelf adjacent to a western boundary current. *Journal of Geophysical Research: Oceans*, 119(8), 4922–4939. <https://doi.org/10.1002/2013jc009735>
- Schiller, A., Oke, P. R., Brassington, G., Entel, M., Fiedler, R., Griffin, D. A., & Mansbridge, J. V. (2008). Eddy-resolving ocean circulation in the Asian-Australian region inferred from an ocean reanalysis effort. *Progress in Oceanography*, 76(3), 334–365. <https://doi.org/10.1016/j.pocean.2008.01.003>
- Sen Gupta, A., McGregor, S., van Sebille, E., Ganachaud, A., Brown, J. N., & Santoso, A. (2016). Future changes to the Indonesian throughflow and Pacific circulation: The differing role of wind and deep circulation changes. *Geophysical Research Letters*, 43(4), 1669–1678. <https://doi.org/10.1002/2016gl067757>
- Shi, G., Ribbe, J., Cai, W., & Cowan, T. (2008). An interpretation of Australian rainfall projections. *Geophysical Research Letters*, 35(2), L02702. <https://doi.org/10.1029/2007gl032436>
- Sprintall, J., Roemmich, D., Stanton, B., & Bailey, R. (1995). Regional climate variability and ocean heat-transport in the Southwest Pacific-Ocean. *Journal of Geophysical Research*, 100(C8), 15865–15871. <https://doi.org/10.1029/95jc01664>
- Steinke, S., Prange, M., Feist, C., Groeneveld, J., & Mohtadi, M. (2014). Upwelling variability off southern Indonesia over the past two millennia. *Geophysical Research Letters*, 41(21), 7684–7693. <https://doi.org/10.1002/2014gl061450>
- Suman, A., Dyer, F., & White, D. (2018). Eastern Australian late Holocene paleotemperature variation inferred from borehole temperature data. *Global and Planetary Change*, 170, 234–245. <https://doi.org/10.1016/j.gloplacha.2018.09.001>
- Suthers, I. M., Young, J. W., Baird, M. E., Roughan, M., Everett, J. D., Brassington, G. B., et al. (2011). The strengthening East Australian current, its eddies and biological effects - An introduction and overview. *Deep-Sea Research Part II*, 58(5), 538–546. <https://doi.org/10.1016/j.dsr2.2010.09.029>
- Ulm, S. (2002). Marine and estuarine reservoir effects in central Queensland, Australia: Determination of Delta R values. *Geoarchaeology*, 17(4), 319–348. <https://doi.org/10.1002/gea.10017>
- Villalba, R., Lara, A., Masiokas, M. H., Urrutia, R., Luckman, B. H., Marshall, G. J., et al. (2012). Unusual southern hemisphere tree growth patterns induced by changes in the southern annular mode. *Nature Geoscience*, 5(11), 793–798. <https://doi.org/10.1038/Ngeo1613>
- Wang, G. J., Cai, W. J., & Purich, A. (2014). Trends in southern hemisphere wind-driven circulation in CMIP5 models over the 21st century: Ozone recovery versus greenhouse forcing. *Journal of Geophysical Research: Oceans*, 119(5), 2974–2986. <https://doi.org/10.1002/2013jc009589>
- Wilson, A. B., Bromwich, D. H., & Hines, K. M. (2016). Simulating the mutual forcing of anomalous high southern latitude atmospheric circulation by El Niño flavors and the Southern Annular Mode. *Journal of Climate*, 29(6), 2291–2309. <https://doi.org/10.1175/Jcli-D-15-0361.1>
- Wörheide, G. (1998). The reef cave dwelling ultraconservative coralline demosponge *Astrosclera willeyana* Lister 1900 from the Indo-Pacific—Morphology, ultrastructure, biocalcification, isotope record, taxonomy, biogeography, phylogeny. *Facies*, 38, 1–88. <https://doi.org/10.1007/Bf02537358>
- Wu, L. X., Cai, W., Zhang, L., Nakamura, H., Timmermann, A., Joyce, T., et al. (2012). Enhanced warming over the global subtropical western boundary currents. *Nature Climate Change*, 2(3), 161–166. <https://doi.org/10.1038/Nclimate1353>
- Wyrtki, K. (1962). The subsurface water masses in the Western South Pacific Ocean. *Marine and Freshwater Research*, 13(1), 18–47. <https://doi.org/10.1071/mf9620018>
- Yan, L. X., Sun, L. G., Wang, Y. H., Huang, W., Qiu, S. C., & Yang, C. Y. (2011). A record of the Southern Oscillation Index for the past 2,000 years from precipitation proxies. *Nature Geoscience*, 4(9), 611–614. <https://doi.org/10.1038/ngeo1231>
- Yang, H., Lohmann, G., Krebs-Kanzow, U., Ionita, M., Shi, X. X., Sidorenko, D., et al. (2020). Poleward shift of the major ocean gyres detected in a warming climate. *Geophysical Research Letters*, 47(5), e2019GL085868. <https://doi.org/10.1029/2019GL085868>
- Yang, H., Lohmann, G., Wei, W., Dima, M., Ionita, M., & Liu, J. P. (2016). Intensification and poleward shift of subtropical western boundary currents in a warming climate. *Journal of Geophysical Research: Oceans*, 121(7), 4928–4945. <https://doi.org/10.1002/2015jc011513>
- Ypma, S. L., van Sebille, E., Kiss, A. E., & Spence, P. (2016). The separation of the East Australian current: A Lagrangian approach to potential vorticity and upstream control. *Journal of Geophysical Research: Oceans*, 121(1), 758–774. <https://doi.org/10.1002/2015jc011133>
- Zhang, J., Liang, M. Q., Li, T. Y., Chen, C. J., & Li, J. Y. (2022). Asian-Australian monsoon evolution over the last millennium linked to ENSO in composite stalagmite delta O-18 records. *Quaternary Science Reviews*, 281, 107420. <https://doi.org/10.1016/j.quascirev.2022.107420>
- Zilberman, N. V., Roemmich, D. H., Gille, S. T., & Gilson, J. (2018). Estimating the velocity and transport of western boundary current systems: A case study of the East Australian current near Brisbane. *Journal of Atmospheric and Oceanic Technology*, 35(6), 1313–1329. <https://doi.org/10.1175/Jtech-D-17-0153.1>

References From the Supporting Information

- Locarnini, R. A., Mishonov, A. V., Baranova, O. K., Boyer, T. P., & Locarnini, R. A. (2019). World ocean atlas, volume 1: Temperature.
- Reimer, P. J., L. Baillie, M. G., Bard, E., Bayliss, A., Beck, J. W., Bertrand, C. J. H., et al. (2004). IntCal04 terrestrial radiocarbon age calibration, 0–26 cal kyr BP. *Radiocarbon*, 46(3), 1029–1058.
- Schlitzer, R. (2021). Ocean data view. Retrieved from odv.awi.de